Industrial Chemistry & Materials

ROYAL SOCIETY OF CHEMISTRY

PAPER

View Article Online
View Journal

Cite this: DOI: 10.1039/d5im00191a

Combustion co-synthesis of nano SiC and purified Si_3N_4 powders by coupling strong and weak exothermic reactions

Lujia Han,[ab] Huakang Zhang,[ab] Xiao Yang,[a] Yuanyuan Li,[c] Yanhao Dong *[c] and Jiangtao Li*[ab]

Silicon carbide (SiC) powders and silicon nitride (Si_3N_4) powders are critical raw materials for advanced ceramic technology and industry. There are two challenges in their synthesis and production: (i) phase formation of nano SiC powders due to harsh reaction temperature and (ii) preparation of high-purity Si_3N_4 powders due to difficulties in removing trace oxygen impurities. Combustion synthesis is a cheap, scalable method for producing SiC and Si_3N_4 powders. However, there are two additional challenges: (iii) combustion synthesis of SiC requires intense external energy input due to the weak exothermic reaction between Si and C and (iv) combustion synthesis of Si_3N_4 requires a diluent to slow down the self-accelerated reaction and fully convert Si to Si_3N_4 due to the strong exothermic reaction between Si and N_2. Here, we reported a new combustion co-synthesis of nano SiC and high-purity Si_3N_4 powders in one chamber, which addressed all four challenges mentioned above: (i) the production of nano SiC powders resolved by fast synthesis, (ii) purified pink-grade Si_3N_4 powders using carbon as an efficient high-temperature oxygen getter, (iii) ignited Si–C combustion by a strongly exothermic Si–N_2 reaction, and (iv) more controllable Si–N_2 combustion with less diluent usage and less residual Si. We demonstrated nano β-SiC powders with ~30 nm primary particle size and high-purity pink-colored β-Si_3N_4 powders with oxygen impurity content down to 0.46 wt%. This study not only offers practical solutions to the production of high-quality SiC and Si_3N_4 powders but also refreshes the design of combustion synthesis with new possibilities and improved controllability.

Received 4th August 2025,
Accepted 9th October 2025

DOI: 10.1039/d5im00191a

rsc.li/icm

Keywords: Combustion synthesis; SiC; Si_3N_4; Nanoparticles; Reaction kinetics.

1 Introduction

The semiconductor industry has undergone rapid development in recent years, resulting in a significant increase in the demand for high-performance SiC and Si_3N_4 ceramics. These ceramics are essential components in semiconductor processing equipment.[1–3] SiC semiconductor components require highly reactive, nanoscale SiC powders to achieve superior mechanical and thermal properties.[4–6] In contrast, high thermal conductivity Si_3N_4 ceramic substrates rely on high-purity and low-oxygen Si_3N_4 powders to ensure optimal thermal conductivity.[7–9] Currently, a variety of synthesis routes, such as carbothermal reduction, sol–gel processing, combustion synthesis, and high-energy ball milling, have demonstrated the capability to successfully produce ceramic powders.[10] In order to produce SiC and Si_3N_4 ceramic powders in a scalable and cost-effective manner, it is essential to consider both manufacturing efficiency and overall material performance.[11,12] In this context, combustion synthesis has emerged as one of the most promising approaches for the large-scale and low-cost fabrication of high-quality Si-based ceramic powders.[13,14] However, existing combustion synthesis technologies for SiC and Si_3N_4 still face critical limitations, highlighting the urgent need for innovation and breakthrough developments.

First, the Si–C reaction system is difficult to sustain in a self-propagating manner due to its low exothermicity (ΔH = −69 kJ mol^{-1}) and relatively low adiabatic combustion temperature (T_{ad} = 1860 °C).[15,16] Previous studies have demonstrated that combustion synthesis of SiC can be achieved through preheating,[17] chemical activation,[18] or nitrogen-assisted catalysis.[19] For instance, the addition of PTFE significantly enhances reactivity through gas-phase

[a] State Key Laboratory of Cryogenic Science and Technology, Technical Institute of Physics and Chemistry, Chinese Academy of Sciences, Beijing 100190, China. E-mail: lijiangtao@mail.ipc.ac.cn
[b] University of Chinese Academy of Sciences, Beijing 100049, China
[c] State Key Laboratory of New Ceramic Materials, School of Materials Science and Engineering, Tsinghua University, Beijing 100084, China. E-mail: dongyanhao@tsinghua.edu.cn

reactions and additional exothermicity.[20] However, these approaches typically involve excessive thermal input to trigger the reaction, which leads to overly high reaction temperatures and consequently causes significant grain coarsening, making it difficult to obtain sub-100 nm SiC powders. Alternatively, mechanically activated combustion synthesis has been employed to enhance reactivity through high-energy ball milling (HEBM), which promotes the formation of nanocomposite Si/C particles.[21] However, the extended mechanical milling of precursors inevitably introduces significant impurities, thereby limiting the purity of the resulting SiC products.[22,23]

Second, although the Si–N_2 system is a highly exothermic reaction (ΔH = −736 kJ mol^{-1}),[15] a large amount of diluents or ammonium salts must be introduced to suppress the reaction temperature in order to prevent the aggregation of molten Si and ensure sufficient nitridation.[24,25] However, such strategies are not without their drawbacks. They result in low net yields and generate corrosive gases, which pose significant environmental concerns.[26] In fact, recent mechanistic studies have shown that the Si–N_2 combustion process follows a vapor–liquid–crystal growth pathway, where the presence of Si_3N_4 diluents not only moderates the temperature but also accelerates combustion front propagation by promoting nucleation of new Si_3N_4 crystals.[27] Therefore, both the combustion synthesis routes for SiC and Si_3N_4 require further optimization and improvement. To optimize the combustion synthesis processes for both types of powders, the guiding principle is to regulate the structure of the combustion wave. Specifically, an appropriate high temperature and high-temperature residence time, imposed on the reactants in the combustion wave region, facilitate precise process control over the nucleation and growth of the target powder products.

Based on the above analysis, this study proposes a simple yet practical strategy for the coupled combustion synthesis of Si–C and Si–N_2 reaction systems. By exploiting the highly exothermic nature of the Si–N_2 reaction in a chemical furnace, the thermal deficit of the weakly exothermic Si–C system can be effectively compensated for. Simultaneously, rapid heat absorption by the Si–C primary reactant system helps suppress overheating in the Si–N_2 zone. By adjusting the ratio between the Si–N_2-based chemical furnace and the Si–C primary reactant system, the temperature field of the coupled reaction can be optimized. This approach aims to simultaneously achieve the synthesis of ultrafine SiC nanoparticles and high-purity Si_3N_4 powders, thereby offering a novel route for the rapid and cost-effective production of advanced SiC and Si_3N_4 ceramic powders.

2 Results and discussion

2.1 Thermodynamic considerations

It is well established that Si_3N_4 powders can be synthesized from Si powder *via* combustion synthesis under high-pressure nitrogen gas. This reaction is highly exothermic, and its adiabatic combustion temperature (T_{ad1}) significantly exceeds the melting point of silicon (T_m = 1410 °C). In order to prevent the melting of Si, which would otherwise reduce the nitridation efficiency, up to 50–60 wt% of Si_3N_4 is typically added as a diluent during the reaction process.[24,28] This addition reduces the adiabatic combustion temperature to a lower level (T_{ad2}) slightly above the melting point of Si (Fig. 1a). However, this approach comes at the cost of a reduced net yield due to the large amount of diluent required. Additionally, for the system of the Si–C reaction, which is weakly exothermic, as demonstrated in Fig. 1b, the adiabatic temperature can be elevated (from T_{ad} to T_{ad+}) by increasing the initial temperature of the system.[22] This provides the necessary thermal conditions to sustain the propagation of the combustion wave in the Si–C system. Nevertheless, such preheating-based strategies inevitably result in prolonged exposure to elevated temperatures, which leads to severe grain coarsening and hinders the formation of nanoscale powders.[29]

In this study, a novel chemical furnace-assisted combustion synthesis approach is proposed for the synthesis of both types of single-phase ceramic powders. In this approach, Si–C and Si–N_2 reaction systems are coupled through a rational powder configuration to synthesize nanoscale SiC powders. During the preheating of the Si–C system by the highly exothermic Si–N_2 reaction, the Si/C primary reactant, which is characterized by high infrared absorption both before and after the reaction, effectively absorbs the radiative heat released from the Si–N_2 reaction, thereby acting as a highly efficient thermal sink. By strategically utilizing this enhanced heat transfer effect, the temperature of the Si–C system can be rapidly elevated to promote its reaction while simultaneously suppressing excessive overheating in the Si–N_2 system. This also enables a reduction in the amount of diluent required in the Si/Si_3N_4 mixture. Thermodynamic calculations reveal that the energy released from the Si–N_2 reaction (~4381 kJ kg^{-1}) vastly exceeds the energy required to ignite the Si/C mixture (~1595 kJ kg^{-1}) by a factor of 2.7 (Note S1). This significant surplus confirms that the Si–N_2 reaction provides ample energy to initiate and sustain the self-propagating combustion process. Based on the above thermodynamic considerations, this study aims to regulate the temperature field of Si–C combustion synthesis by adjusting the ratio between the Si–N_2-based chemical furnace and the Si/C primary reactant system.

2.2 Combustion synthesis and phase formation

The combustion synthesis process for preparing nano-sized SiC assisted by a Si–N_2 chemical furnace is illustrated in Fig. 2a. The heat released from the surrounding Si–N_2 chemical furnace reaction serves to preheat the enclosed Si/C powder mixture. The high temperature at the combustion front of the furnace also provides effective ignition for the Si/C reactants, thereby initiating a self-propagating combustion synthesis reaction. Upon completion of the

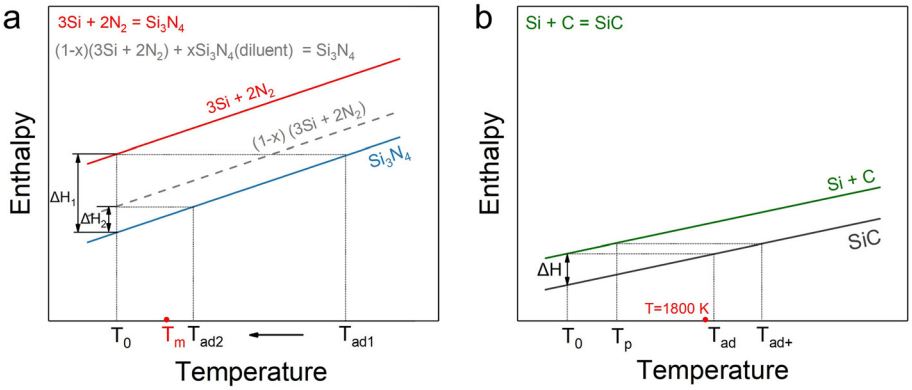

Fig. 1 Schematic illustration of the thermodynamic principles for regulating the adiabatic combustion temperature (T_{ad}) in the Si–C and Si–N_2 combustion synthesis systems. (a) Si–N_2 system and (b) Si–C system.

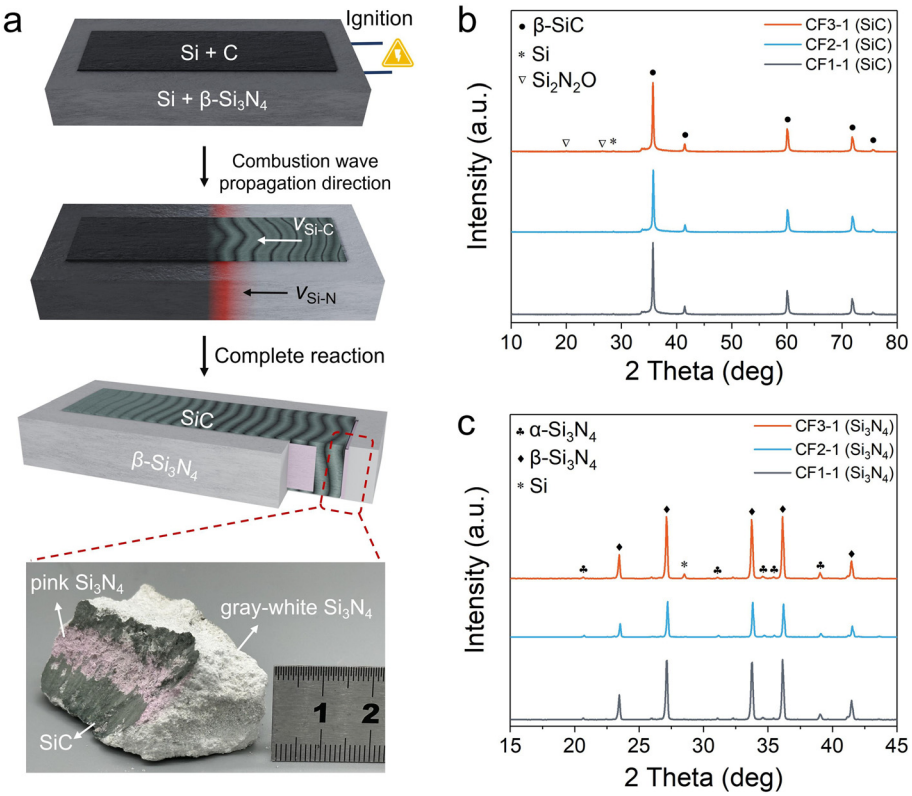

Fig. 2 Reaction mechanism and phase composition of SiC synthesized *via* Si–N_2 chemical furnace-assisted combustion. (a) Schematic of the surrounding chemical furnace-assisted combustion configuration and combustion wave propagation; (b) XRD patterns of the combustion-synthesized product in the central region (primary reaction zone); and (c) XRD patterns of the product in the peripheral region (chemical furnace zone).

reaction, green SiC products were obtained in the central region of the crucible, while the peripheral region yielded gray-white Si_3N_4 products. Notably, a millimeter-thick pink Si_3N_4 interfacial layer was clearly observed at the boundary between the SiC and Si_3N_4 products.

As demonstrated in Fig. 2b, under three distinct chemical furnace conditions with varying Si/Si_3N_4 ratios, all the combustion-synthesized products from the Si–C system exhibited β-SiC as the predominant phase, with a phase content exceeding 99.7 wt%. The minor secondary phases included unreacted residual Si and a trace amount of Si_2N_2O, with the oxygen likely originating from the Si powder itself.[30] In contrast, the reaction products from the three chemical furnace formulations were primarily composed of β-Si_3N_4, accompanied by a small amount of α-Si_3N_4 (Fig. 2c). As is well established, β-Si_3N_4 is a thermodynamically stable phase at high temperatures in comparison with α-Si_3N_4. Consequently, the formation of abundant β-Si_3N_4 indicates

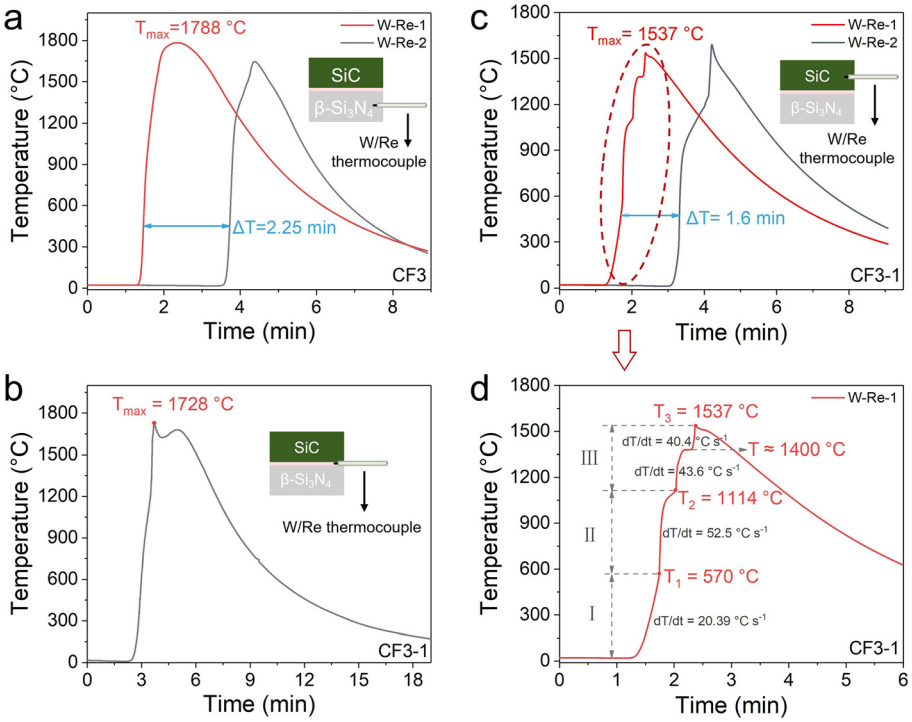

Fig. 3 Temperature–time (*T*–*t*) profiles of the Si–N_2 reaction system, Si–C reaction system, and their interface during chemical furnace-assisted combustion synthesis. (a) *T*–*t* curve of the CF3 chemical furnace system during the reaction process; (b) *T*–*t* curve at the interface between the Si–C and Si–N_2 systems in the CF3-1 reaction configuration; (c) *T*–*t* curve of the Si–C reaction in the CF3-1 system; and (d) enlarged view of the *T*–*t* curve during the Si–C reaction in the CF3-1 system.

that all three furnace systems generated sufficiently high temperatures suitable for triggering the combustion synthesis of the Si–C system.

As illustrated in Fig. 3a–c, the temperature–time profiles were recorded at three different locations during the chemical furnace-assisted combustion synthesis of SiC. The positions of the W/Re thermocouples are indicated in the insets. In the Si–N_2 reaction system, which serves as the chemical furnace, the peak reaction temperatures ranged from 1660 to 1788 °C by adjusting the content of the Si_3N_4 diluent (CF1, CF2, and CF3; Fig. S1 and Table S1). At the interface between the Si–N_2 and Si–C reaction zones, the reaction temperature reached up to 1728 °C. Conversely, the maximum temperature within the Si–C reaction zone exhibited a comparatively lower range, varying from 1086 °C to 1537 °C (Fig. S2). The results obtained demonstrate a rapid radial temperature decrease from the outer Si–N_2 system toward the center. Nevertheless, the combustion wave propagation velocities of the Si–N_2 and Si–C reaction systems were comparable: V_{Si-N} = 16–25 mm min^{-1} and V_{Si-C} = 17–25 mm min^{-1}, respectively. This finding suggests that the combustion wave in the Si–N_2 system effectively initiates and synchronizes the combustion synthesis of the Si–C system. Table 1 provides a synopsis of the combustion wave velocity, peak reaction temperature, and product phase composition of the Si–C system under varying chemical furnace-assisted conditions. It is noteworthy that the Si–C system exhibits characteristics of oscillatory combustion during the synthesis process (Notes S2 and S3). In particular, when a chemical furnace with a high diluent content is utilized (*e.g.*, CF1 with 50 wt%), the Si–C reaction tends to be incomplete.

Table 1 Propagation velocity of combustion wave, peak reaction temperature, and product phase composition of the Si–C system under different chemical furnace-assisted conditions

Reaction systems	*V* (mm min^{-1})	T_{max} (°C)	β-SiC (wt%)	Impurities
CF1-1	17.1	1086	99.8	Si, Si_2N_2O
CF2-1	18.9	1334	99.7	Si, Si_2N_2O
CF3-1	25.4	1537	99.8	Si, Si_2N_2O
CF3-2	13.6	956	—	—
CF3-3	13.6	787	—	—

Using the CF3-1 reaction system as a representative example, Fig. 3d illustrates a magnified view of the *T*–*t* curve for the Si–C region within the CF3-1 chemical furnace-assisted system, with three inflection points along the heating curve marked, along with the corresponding heating rates. Based on this analysis, stage I (T < ~600 °C) corresponds to the preheating of the Si–C system due to heat released from the outer chemical furnace. Stage II (~570–1100 °C) is attributed to the exothermic Si–N_2 reaction. This reaction occurs at such a relatively low temperature due to the nitridation of Si vapor diffusing from the chemical furnace into the Si–C region.[31] The heat released by this vapor-phase Si–N_2 reaction further initiates additional nitridation reactions with the residual raw materials in the Si–C region, thereby accelerating the heating rate to

approximately 52.5 °C s^{-1}. In stage III (T > ~1100 °C), the temperature becomes sufficiently high to trigger the highly exothermic Si–C reaction,[32,33] which is the primary heat source at this stage. This reaction leads to an increase in temperature, which ultimately reaches 1537 °C. The observation of a temperature plateau near 1400 °C can be attributed to the endothermic melting of Si powder.

According to the thermal profile, the critical ignition temperature (T_i) for the combustion synthesis of SiC in this system is estimated to be around 1100 °C, which is approximately 100 °C lower than the value reported by Wang *et al.* for radio-frequency-heated SiC combustion synthesis under an Ar atmosphere (T_i = 1200 °C).[34] This reduction in T_i is likely due to the increased reactivity of the Si reagent, which originates from two primary factors: (1) the diffusion of reactive gaseous Si generated under the strong exothermic conditions of the chemical furnace, and (2) the high-temperature decomposition of newly formed Si_3N_4 in the presence of coexisting carbon in this region, which further releases highly reactive Si vapor.[35,36] Additionally, at approximately 2100 K, the Si vapor pressure over the Si/Si_3N_4 system (≈4×10^{-1} Pa) exceeds that over the Si/SiC system (≈3×10^{-2} Pa) by an order of magnitude, and this disparity in Si vapor pressure between Si_3N_4 and SiC further biases the reaction toward SiC formation under non-equilibrium conditions.[30]

To determine the minimum required amount of chemical furnace material capable of driving the weakly exothermic Si–C reaction, the effect of varying the mass ratio between the chemical furnace reactants and the primary reactants (*i.e.*, $W_{Si/Si_3N_4}:W_{Si/C}$) was investigated based on the CF3 chemical furnace system. The results indicated that when the ratio was reduced from 3 : 1 to 1 : 1, the combustion wave in the Si–C system was unable to propagate over a significant distance, and SiC formation occurred exclusively in proximity to the ignition source. The maximum temperature in the reacted region, as measured by thermocouples, was found to be below 1000 °C (Fig. S3). This observation highlights that the temperature field within the Si–C primary reactant system can be flexibly and conveniently tuned by adjusting the mass ratio between the chemical furnace and the primary reactants. Experimental results indicate that a mass ratio of $W_{Si/Si_3N_4}:W_{Si/C}$ = 3 : 1 is optimal because it ensures that the synthesized SiC experiences a sufficiently high temperature and thermal holding time, resulting in well-dispersed nanoscale SiC powders.

Interestingly, when the chemical furnace-assisted combustion synthesis of SiC was performed, the Si–N_2 system, serving as the chemical furnace, exhibited markedly different behavior compared to when it underwent combustion synthesis independently. As shown in Fig. 4a, the residual Si content in the product of the standalone CF3 furnace was 10.4 wt%. However, when the same CF3 system was used as a chemical furnace to assist SiC synthesis (CF3-1), the residual Si content in the chemical furnace product was significantly reduced to only 1.66 wt%, representing an 84% decrease. A similar trend was observed across other chemical furnace systems with varying diluent contents. Each coupled system exhibited reduced residual Si content in the furnace product. Detailed comparisons of phase compositions are presented in Table S2.

These results demonstrate that the residual Si issue induced by melting during the combustion synthesis of the Si–N_2 system can be substantially mitigated by coupling it with the Si–C system. This improvement is attributed to thermal radiation transfer from the combustion wave zone to the Si–C primary reactant. As illustrated in Fig. 4b, the Si/C powder mixture exhibits high radiative absorptivity, with an infrared emissivity of approximately 0.9. In accordance with the Stefan–Boltzmann law,[37] the radiant energy emitted by a blackbody increases sharply as the temperature increases. The Si/C primary reactant functions as an efficient absorber of this radiative heat, which facilitates the rapid dissipation of heat from the combustion wave zone (the region where Si_3N_4 is formed). Consequently, the primary reactant plays a crucial role in modulating the temperature field of the chemical furnace system. By appropriately harnessing this thermal regulation effect, the synchronous and synergistic

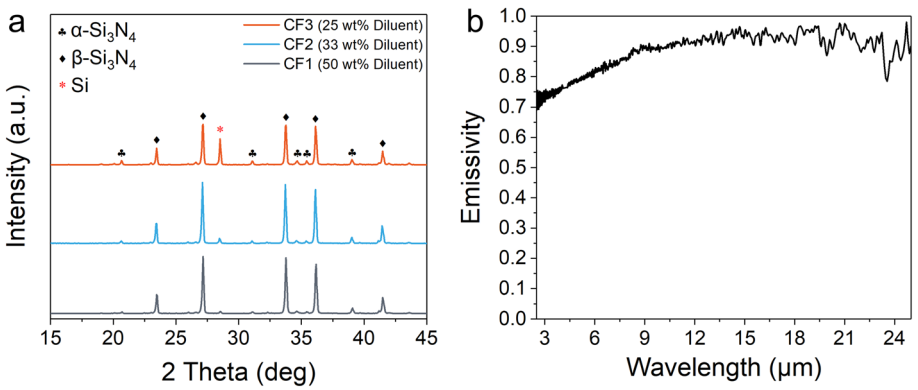

Fig. 4 Phase composition of the products from three Si–N_2 chemical furnace systems and spectral emissivity of the Si/C reactant. (a) XRD patterns of the products obtained from independently reacted chemical furnace systems with varying diluent contents; and (b) infrared emissivity spectrum of the Si/C reactant.

combustion synthesis of the Si–N_2 and Si–C systems can be effectively realized.

2.3 Microstructure of nano SiC

SEM observation of the nano-SiC powders synthesized *via* CF3-1 chemical furnace-assisted combustion revealed that the powders consisted of large aggregates of nano-sized SiC particles. After mild ultrasonic dispersion, the aggregates exhibited a D_{50} of ~780 nm (Fig. S4). This submicron-scale aggregation is acceptable for slurry preparation and coating and can be further reduced by milling to ensure uniformity in subsequent processing. As shown in Fig. 5a, the SiC particles are uniformly distributed across the entire field of view and exhibit an equiaxed crystal morphology. The particle size statistics shown in Fig. 5b indicate that the average diameter of the SiC nanoparticles is approximately 30 nm, which is superior to that achieved by the preheating method (~130 nm)[17] and the electric field-assisted method (on the micrometer scale)[38] and is comparable to those produced by CVD[39] and carbothermal reduction methods,[40] while requiring neither complex equipment nor prolonged reaction time (Table S3). Similar particle sizes and morphological characteristics were observed for the products synthesized in the CF1-1 and CF2-1 systems (Fig. S5). A comparison between the raw carbon black and the synthesized SiC particles revealed that the SiC nanoparticles retained the morphology of the carbon black precursor (Fig. 5c and S6). Selected area electron diffraction (SAED) further confirmed the face-centered cubic (FCC) structure of the SiC nanoparticles. As shown in Fig. 5d, high-resolution TEM (HRTEM) images revealed an interplanar spacing of ~0.25 nm, corresponding to the (111) plane of β-SiC.[41] Stacking faults (SFs) observed in the SiC nanoparticles (Fig. S7) are likely attributed to the non-equilibrium nature of the combustion synthesis process, characterized by high temperatures and rapid heating/cooling rates.[42] Energy-dispersive X-ray spectroscopy (EDS) analysis indicates that a small amount of oxygen is distributed on the surface of the SiC nanoparticles (Fig. S8). In summary, the primary phase of the synthesized nanoparticles is β-SiC. Minor impurities, including residual Si, Si_2N_2O, and surface oxygen, were also detected. The nitrogen content was determined to be ~2.1 wt% by oxygen–nitrogen analysis.

2.4 Microstructural and spectroscopic analysis of pink β-Si_3N_4 in the chemical furnace system

As previously mentioned, a layer of pink Si_3N_4 powder was observed on the Si_3N_4 product side at the interface between the chemical furnace and the primary reaction product. SEM observations of the two differently colored Si_3N_4 powders revealed that the gray-white Si_3N_4 exhibits a more well-developed columnar grain structure, which is a characteristic of β-Si_3N_4 (Fig. 6a and b).[43] This difference in microstructure is likely related to the reaction temperature. The pink Si_3N_4, being adjacent to the Si–C mixed powder, experienced a lower crystal growth temperature, resulting in an underdeveloped columnar morphology. Statistical analysis of particle sizes

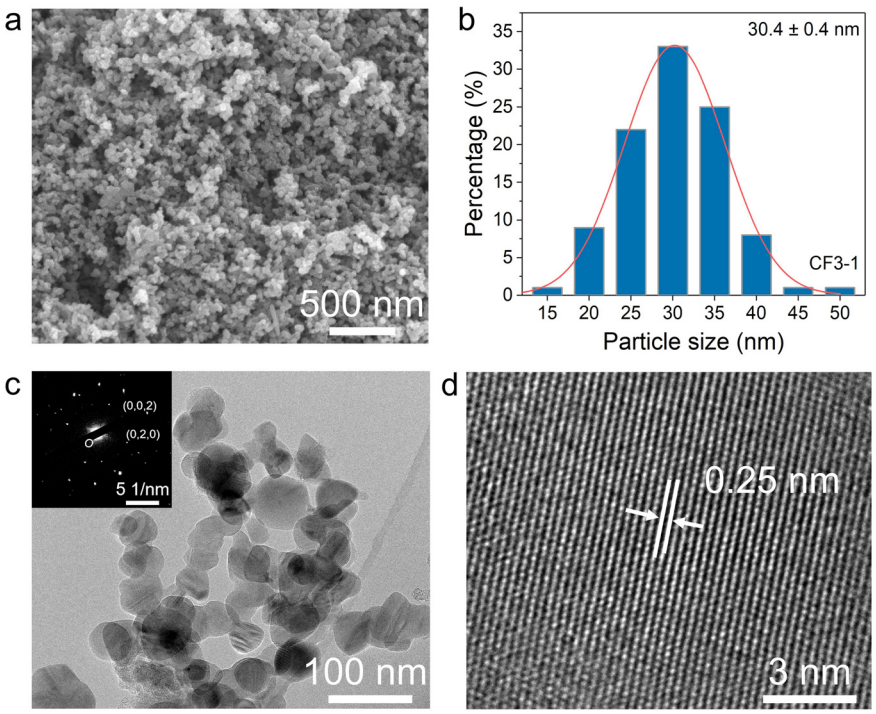

Fig. 5 Microstructure and structural characterization of the nano-SiC synthesized *via* chemical furnace-assisted combustion. (a) SEM image of the combustion-synthesized SiC nanoparticles; (b) statistical particle size distribution of the SiC nanoparticles; (c) TEM image of the SiC nanoparticles (the inset shows the SAED pattern of SiC); and (d) HR-TEM image of the SiC nanoparticles.

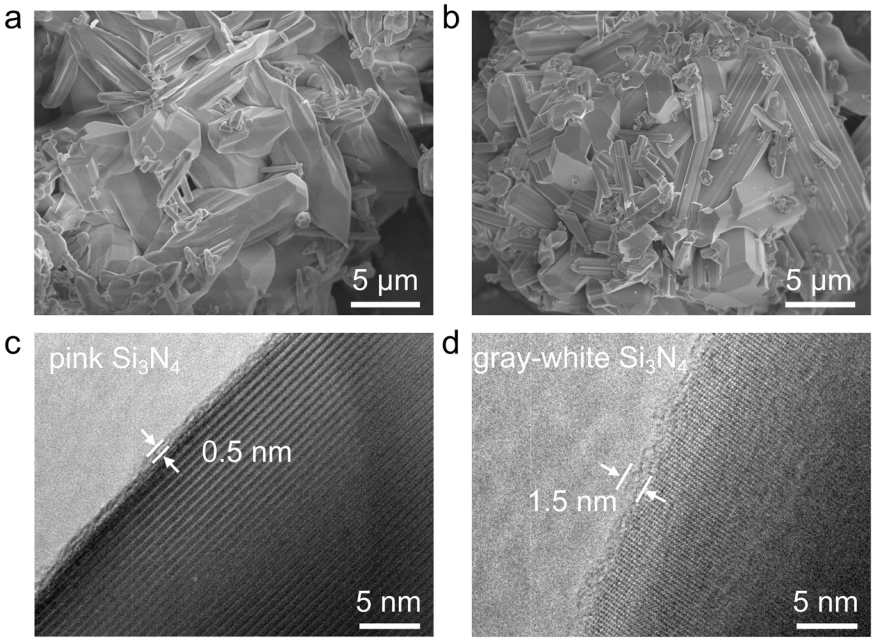

Fig. 6 Microstructures of the combustion-synthesized Si_3N_4 products. (a) SEM image of pink Si_3N_4; (b) SEM image of gray-white Si_3N_4; (c) high-resolution TEM image of pink Si_3N_4; and (d) high-resolution TEM image of gray-white Si_3N_4.

further indicated that the pink Si_3N_4 powder has an average particle size of approximately 4.6 μm, while the gray-white Si_3N_4 powder had a larger average size of about 3.3 μm (Fig. S9). A comparative analysis of the phase composition between the pink and the concurrently generated gray-white Si_3N_4 powders showed that both consist mainly of β-Si_3N_4 (Fig. S10 and Table S4). However, the pink Si_3N_4 contains a lower amount of residual Si, indicating a higher phase purity.

It should be emphasized that the pink β-Si_3N_4 obtained at the reaction interface exhibits a lower oxygen content compared to the gray-white β-Si_3N_4, with the results summarized in Table 2. Furthermore, a comparison with the oxygen content of commercially available high-purity Si_3N_4 powder from the UBE Corporation (Japan) further confirms that the combustion-synthesized Si_3N_4 possesses a lower oxygen concentration. This decrease in oxygen is directly correlated with the thinning of the amorphous SiO_2 surface layer, as confirmed by the TEM observations that the amorphous oxide layer on the surface of the pink Si_3N_4 is less than 1 nm thick, while the oxide layer on the gray-white Si_3N_4 surface measures 1–2 nm in thickness (Fig. 6c and d).

The ultralow oxygen content in the pink Si_3N_4 powder can be explained based on the Ellingham diagram (Fig. 7).[44]

Table 2 Elemental composition analysis of different Si_3N_4 samples

Samples	O (wt%)	N (wt%)	Al (ppm)	Ca (ppm)	Fe (ppm)
Pink β-Si_3N_4	0.46	32.22	72.70	9.52	22.08
Gray-white β-Si_3N_4	0.66	34.55	74.21	70.94	15.72
Pink β-Si_3N_4 (after annealing)	0.61	34.94	—	—	—
β-Si_3N_3 (diluent)	3.01	38.07	600–700	<100	<100
Si_3N_4 from UBE	1.20	38.33	<20	<30	<20

According to the reaction system analysis, the most likely reaction to occur in the Si–C–O system is as follows:

$$Si + O_2(g) = SiO_2, \quad (1)$$

$$2C + O_2(g) = 2CO(g), \quad (2)$$

$$2CO(g) + SiO_2 = Si + 2CO_2(g). \quad (3)$$

According to the Ellingham diagram, SiO_2 is the thermodynamically stable phase below 1600 °C (reaction (1)). However, when the temperature exceeds 1612 °C, carbon from the Si–C reaction system is converted to CO *via* reaction (2). As shown by the temperature measurements in Fig. 3b, the interface between the Si–N_2 and Si–C systems reaches as high as 1728 °C, making reaction (3) inevitable, thereby creating a CO-rich, low equilibrium oxygen partial pressure reducing environment. Furthermore, according to the Ellingham analysis, at the interfacial temperature of 1728 °C, the oxygen partial pressure corresponding to the C/CO equilibrium is as low as approximately 10^{-14} atm, which is significantly lower than that required for the Si/SiO_2 equilibrium ($\sim 10^{-12}$ atm). Under these conditions, the SiO_2 layer present on the surface of Si_3N_4 is reduced (reaction (3)), ultimately yielding high-purity Si_3N_4 with a low oxygen content. At the interface adjacent to the Si/C primary reactant, the proximity to the carbon source results in the highest CO concentration and thus the lowest oxygen content, which explains the formation of the pink Si_3N_4 obtained.

A comparison of Si_3N_4 powders with different colors is shown in Fig. 8a. Interestingly, after a high-temperature

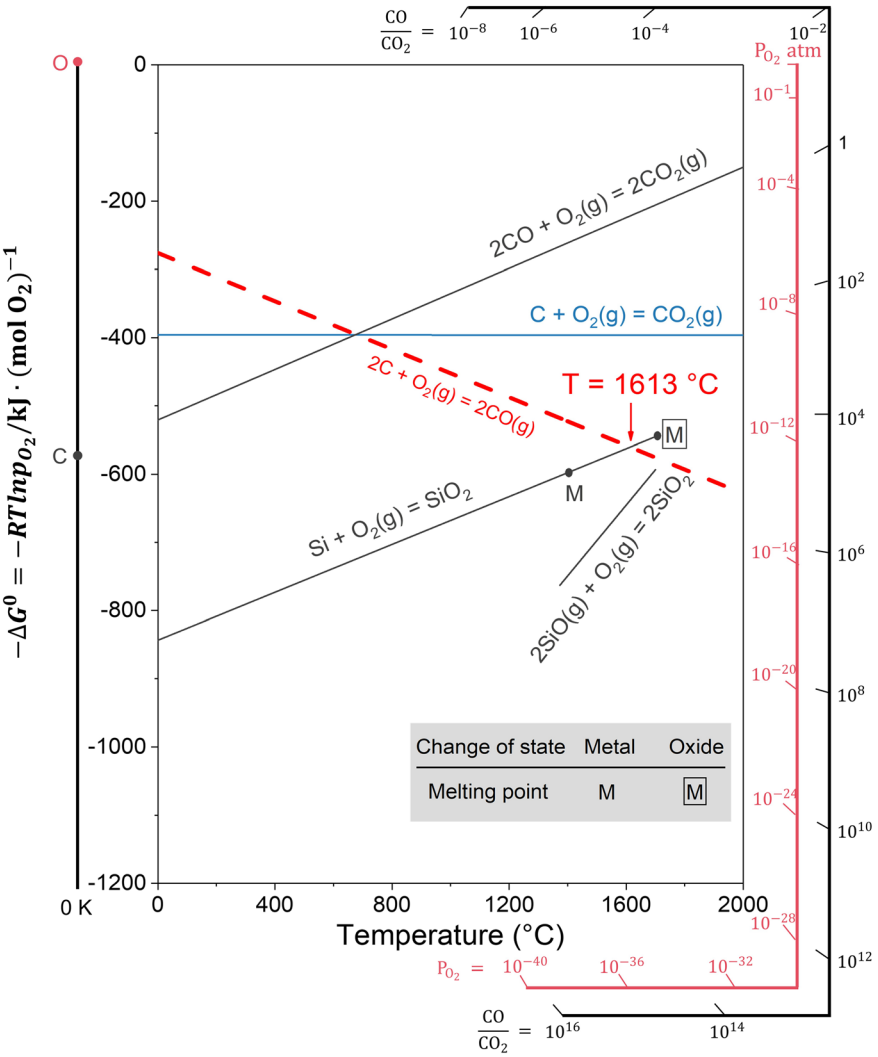

Fig. 7 Thermodynamic analysis of the formation mechanism of high-purity and low-oxygen pink β-Si_3N_4 based on the Ellingham diagram (Si–O and C–O systems).

annealing treatment at 600 °C, the pink β-Si_3N_4 turns gray-white again (Fig. S11). This phenomenon indicates that the surface of the pink Si_3N_4 undergoes oxidation in high-temperature air, resulting in an increased thickness of the oxide layer. Therefore, although the oxygen content itself plays a role, its influence on color difference is essentially

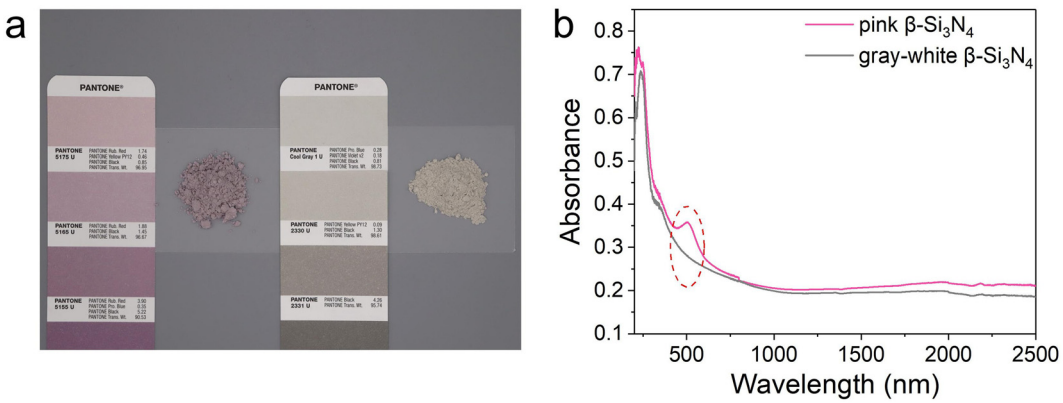

Fig. 8 Color comparison and absorption spectra of the pink and gray-white Si_3N_4 powders. (a) Optical photographs of the two synthesized powder samples compared with Pantone color swatches and (b) UV-vis-NIR absorption spectra of the pink and gray-white Si_3N_4 powders.

Table 3 Design of the reaction systems for chemical furnace-assisted combustion synthesis

Reaction systems	Mass ratio $W_{Si}:W_{Si_3N_4}$ (chemical furnace)	Mass ratio $W_{Si/Si_3N_4}:W_{Si/C}$
CF1-1	1 : 1	3 : 1
CF2-1	2 : 1	3 : 1
CF3-1	3 : 1	3 : 1
CF3-2	3 : 1	2 : 1
CF3-3	3 : 1	1 : 1

manifested through the modulation of the oxide layer thickness. This conclusion is further supported by the band gap (E_g) measurements of β-Si_3N_4 powders of different colors. The absorption spectrum reveals that pink Si_3N_4 exhibits a distinct absorption peak at a visible wavelength of 503 nm (Fig. 8b), which is consistent with the observed pink color. According to the Tauc plot method and using eqn (4),[45,46] the band gap energy (E_g) can be directly calculated from the UV-vis-NIR spectral data:[47]

$$(\alpha h\nu)^{\frac{1}{n}} = C(h\nu - E_g), \quad (4)$$

where α is the absorption coefficient, h is the Planck constant, ν is the photon's frequency, and C is a constant. As shown in Fig. S12, the estimated E_g of pink Si_3N_4 was calculated as 3.87 eV using eqn (4), which is notably lower than that of gray-white Si_3N_4 (4.15 eV). Since the E_g of SiO_2 is larger than that of Si_3N_4, an increase in the thickness of the SiO_2 layer leads to an overall increase in the material's band gap,[48,49] corresponding to the disappearance of the absorption peak at 503 nm and the loss of the pink color. Finally, a comparison of the oxygen and other metallic impurity contents in β-Si_3N_4 and its diluents reveals that the β-Si_3N_4 obtained after combustion synthesis is of higher purity, confirming that the combustion synthesis process has a purification effect on the final product.

The coupled reaction between the Si–N_2 and Si–C systems not only enables efficient preheating and thermal field regulation of the weakly exothermic Si–C reaction *via* the strongly exothermic Si–N_2 system, thereby facilitating the formation of nanoscale SiC at relatively low temperatures, but also benefits from the high infrared absorption of the Si/C powder. This high infrared absorptivity contributes to a reduction in the nitridation temperature and an enhancement in nitridation efficiency. Furthermore, the *in situ* formation of a CO-rich and O_2-deficient reductive atmosphere creates favorable conditions for synthesizing high-purity, low-oxygen Si_3N_4. Consequently, this coupled reaction strategy achieves the simultaneous and synergistic combustion synthesis of nano-SiC and pink, low-oxygen Si_3N_4 ceramic powders.

3 Conclusion

In this study, a coupled combustion synthesis approach was developed by combining a strongly exothermic Si–N_2 system, serving as a chemical furnace, with a weakly exothermic Si–C system as the primary reactant. This strategy enabled the simultaneous and synergistic synthesis of nanoscale SiC and high-purity, low-oxygen, pink β-Si_3N_4 powders.

Thermodynamic analysis of the Si–C–N–O system revealed the formation mechanisms of the ultrafine SiC and pink β-Si_3N_4. The formation of nanoscale SiC was ascribed to the precise regulation of the high-temperature synthesis process. Specifically, the intense exothermic heat release from the Si–N_2 reaction provided the requisite energy input to initiate the combustion synthesis of the weakly exothermic Si–C system. This overcame the challenge of the Si–C system's limited self-propagation ability and capitalized on the transient high-temperature environment induced by the Si–C reaction. Such a transient condition effectively avoids prolonged exposure of reactants to high temperatures, suppresses the grain growth of SiC, and ultimately yields SiC particles with an average primary particle size of approximately 30 nm. This method of generating a transient high-temperature field through the coupling of strong and weak exothermic reactions offers a promising route for the rapid and large-scale fabrication of high-quality nanoscale SiC powders.

The formation of pink, low-oxygen β-Si_3N_4 powder is ascribed to the preferential reaction of residual oxygen in the system and surrounding environment with carbon in the high-temperature combustion wave zone, resulting in the generation of CO. This reaction consequently establishes a localized, oxygen-deficient, and CO-enriched reductive atmosphere at the interface of the Si–N_2 chemical furnace system. Such a reductive environment significantly decreases the oxygen content in the synthesized Si_3N_4 at elevated temperatures. The resultant Si_3N_4 exhibits a distinct pink hue and an ultra-low oxygen content of merely 0.46 wt%, representing a 60% reduction compared to the commercial high-purity Si_3N_4 (1.20 wt%) supplied by the UBE Corporation.

In summary, the proposed strategy of coupling strongly and weakly exothermic reactions enables a complementary reaction pathway for the simultaneous and synergistic synthesis of nanoscale SiC and high-purity, low-oxygen-content Si_3N_4. This work provides a novel and cost-efficient route for the large-scale fabrication of high-quality SiC and Si_3N_4 ceramic powders.

Nevertheless, the scalability of this approach may be limited by temperature gradients affecting product uniformity, and some yield loss is inevitable at the product interface; further optimization is required to ensure reproducibility and industrial feasibility.

4 Experimental section

4.1 Materials

The Si powder (purity: ≥99.999%, D_{50} = 3 μm) was purchased from Fujian Yitian Silicon Industry Co., Ltd. The β-Si_3N_4 powder (purity: ≥99.9%, D_{50} = 1.5 μm) was obtained from Zhongke Xinci (Chongqing) Technology Co., Ltd. Carbon

black (purity: ≥99.9%, D_{50} = 28 nm) was supplied by Shanghai Fluorochem Technology Co., Ltd.

4.2 Synthesis

Combustion synthesis was carried out using a surrounding chemical furnace configuration in which a Si/Si_3N_4 powder mixture served as the chemical furnace reagent, while a Si/C powder mixture acted as the primary reactant. The Si/Si_3N_4 mixture was placed around the Si/C powder in a ring-shaped layout. Specifically, the Si/C primary reactant was placed at the center, while the Si/Si_3N_4 chemical furnace reagent was arranged around it. Three different mass ratios of Si to β-Si_3N_4 (*i.e.*, $W_{Si}:W_{Si_3N_4}$) were prepared for the chemical furnace material: 1 : 1, 2 : 1, and 3 : 1, denoted as CF1, CF2, and CF3, respectively. Specifically, Si powder and β-Si_3N_4 powder (used as the diluent) were weighed according to the designed ratios and ball-milled for 0.5 h to obtain the chemical furnace mixture. For the primary reactant, Si powder and carbon black were mixed at a molar ratio of 1 : 1, with ethanol used as the milling medium. The mixture was then ball-milled at 360 rpm for 4 h using a planetary ball mill to obtain the Si/C composite powder. In the surrounding configuration, a defined mass of the Si/Si_3N_4 furnace material was uniformly arranged around the Si/C powder. The mass ratio between the chemical furnace reagent and the primary reactant ($W_{Si/Si_3N_4}:W_{Si/C}$) was varied among 3 : 1, 2 : 1, and 1 : 1. The detailed compositions and abbreviations of all reaction systems are summarized in Table 3.

After loading, C-type W-Re5/26 thermocouples (ϕ = 0.5 mm × 80 mm) were fixed at the designated measurement point and connected to a four-channel data acquisition system (the maximum acquisition rate is not less than 10 ms each time). The assembled reactants were then placed into a high-pressure reactor, evacuated, and filled with nitrogen gas at a pressure of 3 MPa. The combustion reaction was initiated by passing a 50 A current through a tungsten wire coil embedded at one end of the Si/Si_3N_4 chemical furnace material to trigger the Si–N_2 reaction.

4.3 Characterizations

The microstructures of all samples were characterized by scanning electron microscopy (SEM; S-4800, Hitachi, Japan) and transmission electron microscopy (TEM; JEM F200, JEOL, Japan). Image analysis software (ImageJ) was used to measure the primary particle sizes of over 100 particles in order to calculate the average sizes and size distributions. The phases were characterized by X-ray diffraction (XRD; D8 Focus, Bruker, Germany). The wave velocity (V) was determined by measuring the distance between the two thermocouples and the time difference (Δt) of the combustion wave passing through them. The particle size distributions of the SiC samples were analyzed using a particle size analyzer (Zetasizer Nano ZSE, Malvern, United Kingdom). The particle size distributions of the Si_3N_4 samples were analyzed using a laser particle size analyzer (Bettersize 2000E, Dandong Bettersize, China). Oxygen and nitrogen contents in the sample were measured using an oxygen–nitrogen analyzer (EMGA-820, HORIBA, Japan). The contents of iron, aluminum, and calcium in the sample were measured using an inductively coupled plasma optical emission spectrometer (ICP-OES; 5800, Agilent, USA). The absorption intensities of the sample in the ultraviolet, visible, and near-infrared spectral ranges were measured using an ultraviolet-visible-near-infrared (UV-vis-NIR) spectrometer (Cary 7000, Agilent, USA).

Conflicts of interest

The authors declare that they have no known competing financial interests or personal relationships that could have appeared to influence the work reported in this paper.

Data availability

The data supporting this article are available within the article and its supplementary information (SI). If necessary, the raw data are available from the corresponding authors (Prof. Yanhao Dong and Prof. Jiangtao Li) upon reasonable request.

Supplementary information is available. See DOI: **https://doi.org/10.1039/d5im00191a**.

Acknowledgements

This work was supported by the National Natural Science Foundation of China (U24A2049 and 92263205).

References

1 H. Tanaka, Silicon carbide powder and sintered materials, *J. Ceram. Soc. Jpn.*, 2011, **119**, 218–233.
2 Y. Wang, S. Dong, X. Li, C. Hong and X. Zhang, Synthesis, properties, and multifarious applications of SiC nanoparticles: A review, *Ceram. Int.*, 2022, **48**, 8882–8913.
3 S. Zhao, S. Du, S. Zhang, D. Zhao, B. Fan, B. Wang, F. Li, K. Chen and G. Liu, Low-temperature rapid sintering for the fabrication of biphasic Si_3N_4 ceramics with outstanding mechanical properties, *J. Adv. Ceram.*, 2025, **14**, 9221044.
4 H. Li and J. Sun, Highly selective photocatalytic CO_2 reduction to CH_4 by ball-milled cubic silicon carbide nanoparticles under visible-light irradiation, *ACS Appl. Mater. Interfaces*, 2021, **13**, 5073–5078.
5 F. Nava, G. Bertuccio, A. Cavallini and E. Vittone, Silicon carbide and its use as a radiation detector material, *Meas. Sci. Technol.*, 2008, **19**, 102001.
6 R. A. Andrievski, Nano-sized silicon carbide: Synthesis, structure and properties, *Russ. Chem. Rev.*, 2009, **78**, 821–831.
7 Q. Qin, L. Han, G. Xiong, Z. Guo, J. Huang, Y. Zhang and Z. Shen, Impact of sintering aid type and content on the mechanical properties of digital light processing 3D-printed Si_3N_4 ceramics, *Materials*, 2024, **17**, 5830.

8 M. Kitayama, K. Hirao, A. Tsuge, K. Watari, M. Toriyama and S. Kanzaki, Thermal conductivity of β-Si_3N_4: II, Effect of lattice oxygen, *J. Am. Ceram. Soc.*, 2000, **83**, 1985–1992.
9 H. Shao, J. Qiu, X. Liu, X. Hou and J. Zhang, The temperature-dependent thermal conductivity of C- and O-doped Si_3N_4: First-principles calculations, *Crystals*, 2024, **14**, 549.
10 W. Zhang, An overview of the synthesis of silicon carbide-boron carbide composite powders, *Nanotechnol. Rev.*, 2023, **12**, 20220571.
11 Z. Huang, B. Liang, D. Jiang and S. Tan, Preparation of nanocrystal SiC powder by chemical vapour deposition, *J. Mater. Sci.*, 1996, **31**, 4327–4332.
12 Y. Lan, C. Yin, Y. Huang and L. Zhou, Synthesis of sub-micron spherical α-Si_3N_4 powder by direct nitridation of silicon saw dust, *Silicon*, 2022, **14**, 475–479.
13 J. Narayan, R. Raghunathan, R. Chowdhury and K. Jagannadham, Mechanism of combustion synthesis of silicon carbide, *J. Appl. Phys.*, 1994, **75**, 7252–7257.
14 F. Li, J. Zhang, Y. Ge, K. Chen and G. Liu, Macro synthesis of SiC nanopowders via gas-phase reaction initiated by solid-phase reactants vaporizing in combustion synthesis, *J. Mater. Res. Technol.*, 2025, **35**, 5746–5754.
15 C. Agrafiotis, J. Lis, J. Puszynski and V. Hlavacek, Combustion synthesis of silicon nitride-silicon carbide composites, *J. Am. Ceram. Soc.*, 1990, **73**, 3514–3517.
16 S. Agathopoulos, Combustion synthesis of ultra-fine SiC powders in low pressure N_2-atmosphere, *Ceram. Int.*, 2012, **38**, 4165–4171.
17 R. Pampuch, L. Stobierski and J. Lis, Synthesis of sinterable beta-SiC powders by a solid combustion method, *J. Am. Ceram. Soc.*, 1989, **72**, 1434–1435.
18 G. Liu, K. Yang, J. Li, K. Yang, J. Du and X. Hou, Combustion synthesis of nanosized β-SiC powder on a large scale, *J. Phys. Chem. C*, 2008, **112**, 6285–6292.
19 A. Mukasyan, Y. Lin, A. Rogachev and D. Moskovskikh, Direct combustion synthesis of silicon carbide nanopowder from the elements, *J. Am. Ceram. Soc.*, 2013, **96**, 111–117.
20 A. Mukasyan, Combustion synthesis of silicon carbide, in *Properties and Applications of Silicon Carbide*, ed. R. Gerhardt, InTech, Rijeka, Croatia, 2011, pp. 389–409.
21 D. Moskovskikh, Y. Song, S. Rouvimov, A. Rogachev and A. Mukasyan, Silicon carbide ceramics: Mechanical activation, combustion and spark plasma sintering, *Ceram. Int.*, 2016, **42**, 12686–12693.
22 Y. Yang, K. Yang, Z. Lin and J. Li, Mechanical-activation-assisted combustion synthesis of SiC, *Mater. Lett.*, 2007, **61**, 671–676.
23 H. Jin, J. Li, M. Cao and S. Agathopoulos, Influence of mechanical activation on combustion synthesis of fine silicon carbide (SiC) powder, *Powder Technol.*, 2009, **196**, 229–232.
24 F. Li, W. Cui, Z. Tian, J. Zhang, S. Du, Z. Chen, S. Zhang, K. Chen and G. Liu, Effect of the diluent on combustion synthesis of silicon nitride, *Int. J. Appl. Ceram. Technol.*, 2022, **19**, 2957–2962.
25 L. Wang, G. He, X. Wu, Q. Meng, S. Deng, Z. Yang and J. Li, Effect of Si particle size and NH_4Cl additive on combustion synthesis of α-Si_3N_4, *Ceram. Int.*, 2019, **45**, 21635–21639.
26 J. Zhang, Y. Ge, Z. Tian, S. Sun, W. Cui, G. Liu and K. Chen, Combustion synthesis of α-Si_3N_4 with green additives, *Ceram. Int.*, 2019, **45**, 6594–6596.
27 A. Mukasyan, Combustion synthesis of nitrides: Mechanistic studies, *Proc. Combust. Inst.*, 2005, **30**, 2529–2535.
28 I. Cano, I. Borovinskaya, M. Rodriguez and V. Grachev, Effect of dilution and porosity on self-propagating high-temperature synthesis of silicon nitride, *J. Am. Ceram. Soc.*, 2002, **85**, 2209–2211.
29 J. Zeng, Y. Miyamoto and O. Yamada, Combustion synthesis of Si_3N_4-SiC composite powders, *J. Am. Ceram. Soc.*, 1991, **74**, 2197–2200.
30 O. Yamada, K. Hirao, M. Koizumi and Y. Miyamoto, Combustion synthesis of silicon carbide in nitrogen atmosphere, *J. Am. Ceram. Soc.*, 1989, **72**, 1735–1738.
31 R. Ghoshtagore and R. Coble, Self-diffusion in silicon carbide, *Phys. Rev.*, 1966, **143**, 623–626.
32 V. Gorovenko, V. Knyazik and A. Shteinberg, High-temperature interaction between silicon and carbon, *Ceram. Int.*, 1993, **19**, 129–132.
33 R. Pampuch, E. Walasek and J. Bialoskórski, Reaction mechanism in carbon-liquid silicon systems at elevated temperatures, *Ceram. Int.*, 1986, **12**, 99–106.
34 L. Wang, Y. Peng, X. Hu and X. Xu, Combustion synthesis of high purity SiC powder by radio-frequency heating, *Ceram. Int.*, 2013, **39**, 6867–6875.
35 H. Wang and G. S. Fischman, In situ synthesis of silicon carbide whiskers from silicon nitride powders, *J. Am. Ceram. Soc.*, 1991, **74**, 1519–1522.
36 G. Liu, K. Chen and J. Li, Combustion synthesis of carbide powders, in *Combustion Synthesis*, 2025, pp. 299–346.
37 A. Kolesnichenko, Thermodynamics of the Bose gas and blackbody radiation in non-extensive Tsallis statistics, *Sol. Syst. Res.*, 2020, **54**, 420–431.
38 A. Feng and Z. Munir, The effect of an electric field on self-sustaining combustion synthesis: Part II. Field-assisted synthesis of β-SiC, *Metall. Mater. Trans. B*, 1995, **26B**, 587–593.
39 Y. Kamlag, A. Goossens, I. Colbeck and J. Schoonman, Laser CVD of cubic SiC nanocrystals, *Appl. Surf. Sci.*, 2001, **184**, 118–122.
40 M. Sharma, R. Upadhyay, S. Amritphale and N. Chandra, Synthesis of nano-structured 3C-SiC by carbothermal reduction of silicon bearing gel and carbon soot, *Mater. Lett.*, 2011, **65**, 2161–2164.
41 L. Han, S. Chen, H. Li, Y. Dong, C. Wang and J. Li, Rapid and inexpensive synthesis of liter-scale SiC aerogels, *Nat. Commun.*, 2024, **15**, 6959.
42 F. Li, W. Cui, Z. Tian, J. Zhang, S. Du, Z. Chen, K. Chen and G. Liu, Controlled growth of SiC crystals in combustion synthesis, *J. Am. Ceram. Soc.*, 2022, **105**, 44–49.
43 S. Chen, L. Han, J. Li, Y. Dong and C. Wang, Rapid synthesis of high-strength porous Si_3N_4 ceramics based on

spontaneous solidification of multi-phase particles, *J. Am. Ceram. Soc.*, 2025, e20441.

44 H. Ellingham, Reducibility of oxides and sulphides in metallurgical processes, *J. Chem. Technol. Biotechnol.*, 1944, **63**, 125–160.

45 J. Tauc, R. Grigorovici and A. Vancu, Optical properties and electronic structure of amorphous germanium, *Phys. Status Solidi*, 1966, **15**, 627–637.

46 P. Praus, O. Kozák, K. Kočí, A. Panáček and R. Dvorský, CdS nanoparticles deposited on montmorillonite: Preparation, characterization and application for photoreduction of carbon dioxide, *J. Colloid Interface Sci.*, 2011, **360**, 574–579.

47 P. Jubu, O. Obaseki, A. Nathan-Abutu, F. Yam, Y. Yusof and M. Ochang, Dispensability of the conventional Tauc's plot for accurate bandgap determination from UV–Vis optical diffuse reflectance data, *Res. Opt.*, 2022, **9**, 100273.

48 A. Tsaturyan, E. Kachan, R. Stoian and J. Colombier, Unraveling the electronic properties in SiO_2 under ultrafast laser irradiation, *npj Comput. Mater.*, 2024, **10**, 200.

49 M. Sarki, I. Echi, A. Amah, I. Ahemen, K. Chan, U. Rilwan and M. Sayyed, Structural, electronic and optical properties of α-Si_3N_4, β-Si_3N_4 and γ-Si_3N_4 using density functional theory, *Next Research*, 2024, **1**, 100048.